THE ASTROPHYSICAL JOURNAL, 306:L101–L104, 1986 July 15

INFRARED CIRRUS AND HIGH-LATITUDE MOLECULAR CLOUDS

JANET L. WEILAND
University of Maryland; and Applied Research Corporation
LEO BLITZ[1]
University of Maryland
ELI DWEK AND M. G. HAUSER
Laboratory for Extraterrestrial Physics, Goddard Space Flight Center
LORIS MAGNANI
University of Maryland
AND
LEE J. RICKARD
Sachs-Freeman Associates; and E. O. Hulburt Center for Space Research, Naval Research Laboratory
Received 1986 March 3; accepted 1986 April 18

ABSTRACT

We establish that a close correlation exists between far-infrared "cirrus" emission observed with *IRAS* and the CO emission from high-latitude molecular clouds (HLCs). In all cases, the HLCs correspond to the central portions of 100 μm infrared cirrus features. This association firmly establishes at least some of the cirrus as features of the local interstellar medium with typical distances of 100 pc. The infrared energy distribution of the cirrus displays an excess of 12 and 25 μm emission over that expected from dust at equilibrium temperature, consistent with emission from very small (< 10 Å) transiently heated grains.

Subject headings: infrared: general — interstellar: grains — interstellar: matter

I. INTRODUCTION

Among the unexpected results from the *Infrared Astronomical Satellite* (*IRAS*) was the discovery of large-scale, extended filamentary emission at 60 and 100 μm, described as "infrared cirrus" by Low *et al.* (1984). They identified several cirrus features with prominent H I clouds but noted the presence of cirrus at some places without prominent H I, and vice-versa. Subsequent investigators have identified other regions of correlated H I and infrared cirrus and noted that cirrus emission is also visible at 12 and 25 μm. It has been suggested that the surprising short wavelength emission arises from very small grains or large polycyclic aromatic molecules (e.g., Boulanger, Baud, and van Albada 1985; Puget, Leger, and Boulanger 1986; Draine and Anderson 1985).

Concurrent with the discovery of the *IRAS* cirrus, Blitz, Magnani, and Mundy (1984, hereafter BMM) reported the detection of a large number of high galactic latitude ($|b| \geq 25°$) molecular clouds not previously cataloged. Maps of these molecular clouds (Magnani, Blitz, and Mundy 1985, hereafter MBM) show a range of morphologies with extents sometimes exceeding 10°. On the basis of the large angular sizes of the CO clouds, BMM suggested that the *IRAS* cirrus could be emission from high latitude molecular clouds (HLCs). We have compared the MBM and *IRAS* data and find that in all instances these HLCs are associated with *IRAS* 100 μm cirrus emission. In the following sections, we will briefly describe how the IR and CO data bases were compared and demonstrate the correlation between several representative CO clouds and the corresponding infrared cirrus features. We also discuss the physical properties of the dust clouds and implications for various models of interstellar grains.

II. DESCRIPTION OF THE DATA

MBM mapped 23 CO cloud complexes at sampling intervals of 10′ and 20′ (FWHM of beam = 2′.3). The velocity-integrated CO antenna temperatures for each cloud, W(CO), have been interpolated onto the same grid as the *IRAS* HCON 3 Sky Flux plates, which are 16°.5 × 16°.5 mosaics of the sky with 6′ resolution and 2′ pixels (*IRAS Explanatory Supplement* 1984). Additional data on some of the HLCs is available in the form of estimates of the extinction (A_v) derived from star counts, and 21′ resolution H I observations (Magnani and de Vries 1986; Magnani, Blitz, and Wouterloot 1986).

Zodiacal emission was removed from the *IRAS* images by subtracting a locally determined, two-dimensional linear background. The determination of the cirrus emission at 12 and 25 μm is complicated by the striping noise in the *IRAS* data products and the large (> 95%) contribution of the zodiacal emission to the extended source signal at these wavelengths. Thus, cirrus intensities at 12 and 25 μm, though representing definite detections, have relatively large uncertainties.

For each CO cloud mapped by MBM, the *IRAS* 100 μm image shows cirrus of similar structure. In particular, there is

[1]Alfred P. Sloan Foundation Fellow.

close correspondence between the 100 μm cirrus emission peaks and the CO intensity peaks. Corresponding cirrus emission is also present at 60 μm and is often faintly seen at 12 and 25 μm. For detailed study, we have selected three MBM clouds of differing morphological types. Cloud 16 is a large (2° × 3°) amorphous structure south of the Taurus dark clouds. Cloud 20 (L1642) exhibits a centrally condensed structure and is of special interest because of the reported presence of at least one pair of T Tauri stars near the center of the cloud (G. Sandell *et al.*, in preparation). Cloud 30 is part of a long filamentary complex associated with a large looplike structure near the north ecliptic pole. The loop is especially visible at 100 μm, and also has a counterpart in the Heiles and Habing (1974) H I survey, as well as having associated optical reflection (Sandage 1976).

III. RESULTS

Figures 1*a*–1*c* (Plate L2) depict the 100 μm *IRAS* images of the cirrus corresponding to MBM clouds 16, 20, and 30. The 100 μm images are overlayed with the MBM CO contours and show a clear correspondence between the CO and 100 μm emission features. The 100 μm cirrus emission is, however, more extensive than the lowest CO contour. Although this may be partly due to CO detection limits, the more extended 100 μm emission is associated with H I emission that occurs well beyond the limits of the CO. This is seen in Figure 1*d*, which shows the H I emission (Magnani, Blitz, and Wouterloot 1986) in a narrow velocity range centered on the CO velocity (there is little background gas at this velocity). The existence of infrared cirrus emission from clouds containing H I but not H_2 is also indicated by the nondetection of CO in the original cirrus features identified by Low *et al.* (1984) (MBM; Keto and Myers 1986).

Measurements of the *IRAS* 12, 25, 60, and 100 μm intensities above local background levels have been made for selected regions within the three clouds. Table 1A lists peak infrared intensities (typically averaged over a 10′ by 10′ region), the location of the center of the averaging rectangle, and corresponding average values of W(CO) (from MBM) and A_v (Magnani and de Vries 1986). Peak locations were chosen from the 100 μm images. Table 1B lists infrared intensities, W(CO), and A_v averaged over larger rectangular regions centered within the outermost CO contours.

IV. DISCUSSION

The predominantly molecular high-latitude clouds are cores of infrared cirrus features. We thus adopt for these cirrus clouds the average properties of the ensemble of HLCs studied by MBM. This implies that they are features of the local ISM, with distances ~ 100 pc (BMM; Magnani and de Vries 1986), sizes ~ 2 pc, ages < 10^6 yr, and masses ~ 50 $M_\odot$.

In spite of their different morphologies, the three clouds we have analyzed have rather similar dust properties. Table 2A

TABLE 1

OBSERVED CLOUD PROPERTIES

A. CLOUD PROPERTIES AT PEAKS

Cloud	Peak	Peak Area	Location of Peak Center α(1950)	δ(1950)	I_ν (MJy sr^{-1})[a,b] 12 μm	25 μm	60 μm	100 μm	W(CO)[c] (K km s^{-1})	A_v[b] (mag)	Comment
16......	1	10′ × 10′	03ʰ20ᵐ57ˢ6	12°31′02″	0.5 ± 0.3	0.4 ± 0.1	2.3 ± 0.2	16.8 ± 1.2	1.4 ± 0.2	0.5 ± 0.2	
	2	10 × 10	03 21 19.7	10 45 43	0.7 ± 0.2	0.6 ± 0.1	3.1 ± 0.2	19.1 ± 0.8	2.6 ± 0.4	1.0 ± 0.1	
	3	10 × 10	03 17 35.3	11 04 27	0.5 ± 0.2	0.3 ± 0.5	3.3 ± 0.3	19.2 ± 1.7	2.8 ± 0.4	0.8 ± 0.1	Noisy 25 μm
	4	10 × 10	03 15 27.0	11 20 47	0.8 ± 0.3	0.5 ± 0.2	2.9 ± 0.2	18.1 ± 0.8	...[d]	1.0 ± 0.1	
	5	8 × 10	03 17 10.0	11 42 18	0.5 ± 1.2	0.6 ± 0.7	2.6 ± 0.3	15.5 ± 1.0	...[d]	0.4 ± 0.1	Point source contaminated at 12 μ; noisy 25 μm
20......	1	8 × 12	04 33 33.9	−14 45 20	0.4 ± 0.1	0.4 ± 0.2	2.1 ± 0.2	14.0 ± 0.8	3.2 ± 0.5	1.0 ± 0.1	
	2	10 × 12	04 31 47.4	−14 16 44	0.5 ± 0.1	0.4 ± 0.2	1.7 ± 0.1	12.6 ± 1.0	6.3 ± 0.9	1.2 ± 0.2	
	3	10 × 10	04 32 44.0	−14 20 08	0.6 ± 0.4	0.5 ± 0.6	2.0 ± 0.9	12.8 ± 1.4	6.8 ± 1.0	1.5 ± 0.2	Point source contaminated—position of T Tau stars?
30......	1	10 × 14	09 24 42.1	70 45 10	0.4 ± 0.3	0.3 ± 0.1	1.2 ± 0.2	8.5 ± 1.1	3.4 ± 0.5	...[d]	
	2	12 × 18	09 22 49.4	69 39 04	0.4 ± 0.1	0.5 ± 0.3	1.1 ± 0.2	6.7 ± 0.8	3.4 ± 0.5	...[d]	

B. AVERAGE CLOUD PROPERTIES

Cloud	Averaging Area (sq. degrees)	I_ν (MJy sr^{-1})[a,b] 12 μm	25 μm	60 μm	100 μm	W(CO)[c] (K km s^{-1})	A_v[b] (mag)
16.......	6.5	0.4 ± 0.2	0.3 ± 0.1	2.3 ± 0.4	13.9 ± 2.2	1.3 ± 0.2	0.6 ± 0.3
20.......	1.8	0.4 ± 0.1	0.3 ± 0.1	1.4 ± 0.3	8.1 ± 2.2	2.2 ± 0.3	0.8 ± 0.2
30.......	1.2	0.2 ± 0.1	0.2 ± 0.1	0.8 ± 0.3	4.8 ± 1.6	1.6 ± 0.2	...[d]

[a]All *IRAS* intensities are background subtracted and color corrected using a 240 K blackbody (*IRAS Explanatory Supplement*, Table VI C.6).
[b]Errors are 1σ statistical standard deviation of mean.
[c]Errors are 15% systematic errors.
[d]No data (or insufficient data).

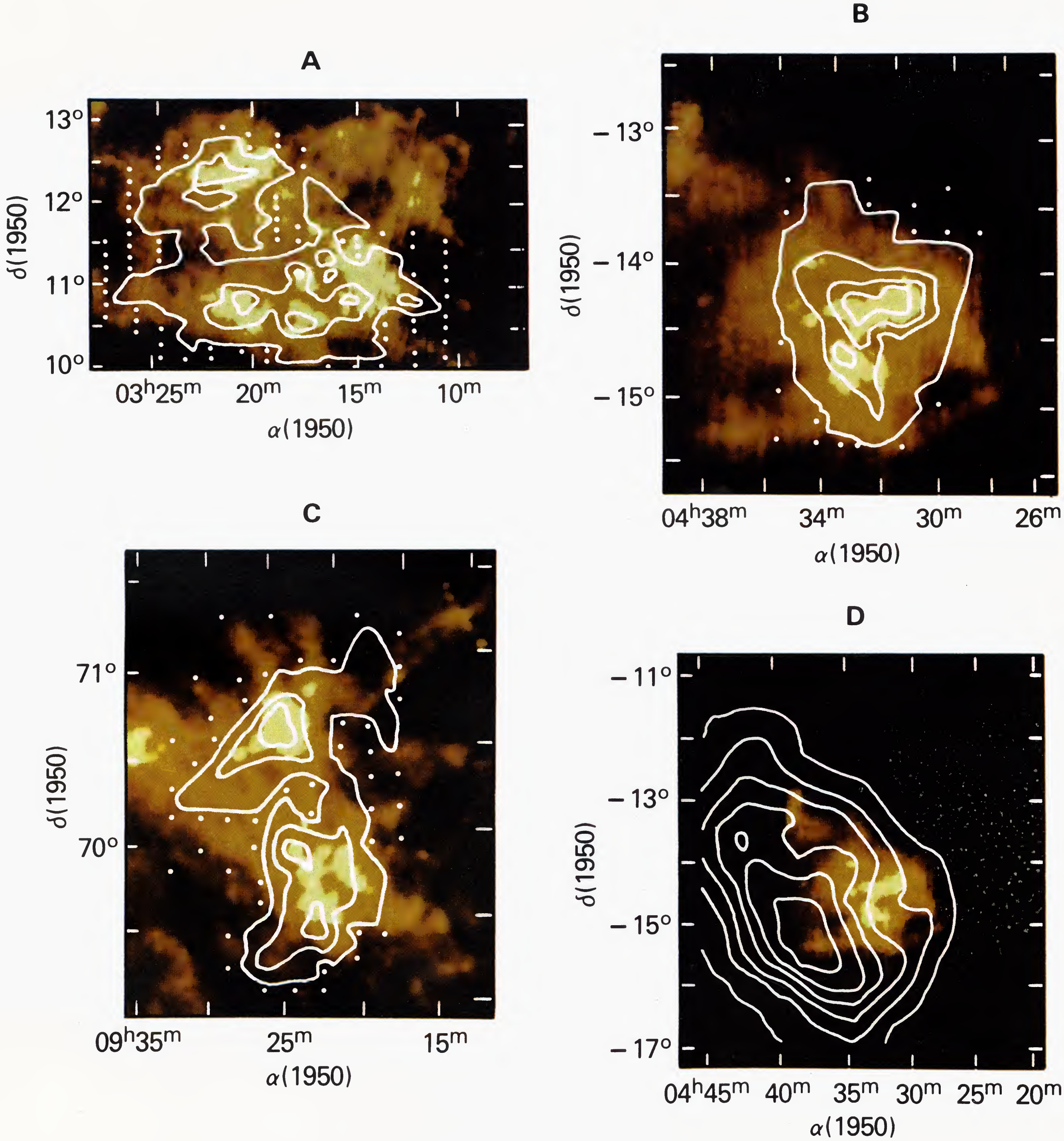

FIG. 1.—*IRAS* 100 μm images (HCON3) of MBM clouds 16, 20, and 30 (after background removal). Black corresponds to background levels; white to peak 100 μm intensity. (*a*) Cloud 16 100 μm image overlaid with W(CO) contours at levels 0.5, 2.25, and 3.75 K km s^{-1}. Small white dots located outside the lowest CO contour indicate positions where MBM observed, but did not detect, CO emission. (*b*) Same as (*a*) for Cloud 20; the W(CO) contour levels are 0.5, 2.25, 3.75, and 5.75 K km s^{-1}. (*c*) Same as (*a*) for Cloud 30. (*d*) Cloud 20 100 μm image overlaid with H I contours at levels 5, 10, 15, 20, 25, and 30 K. H I is the average antenna temperature between −1 and +1 km s^{-1}.

WEILAND *et al.* (*see* page L102)

TABLE 2

AVERAGE DERIVED PROPERTIES

A. SINGLE DUST TEMPERATURE MODEL

Cloud	T_d(K)[a]	τ_{100}[b]	A_v/τ_{100}
16	23	2×10^{-4}	~ 2900
20	23	1×10^{-4}	~ 7100
30	23	7×10^{-5}	. . .[c]
Clouds A–D (Low *et al.*)	24	5×10^{-5}	~ 2500

B. STOCHASTIC HEATING MODEL[d,e]

Cloud	τ_{100}	$M_d(M_\odot)$	$L_{IR}(L_\odot)$	PAH[f] Abundance
16......	7.4×10^{-4}	1.3	330	. . .
	2.7×10^{-4}	0.5	91	1.8×10^{-3}
20......	4.3×10^{-4}	0.2	53	. . .
	3.0×10^{-4}	0.1	28	2.8×10^{-3}
30......	2.6×10^{-4}	0.09	22	. . .
	1.7×10^{-4}	0.06	13	2.1×10^{-3}

[a] Physical dust temperature derived from I_{60}/I_{100} and emissivity varying as $\nu^{1.5}$.

[b] Derived from T_d and I_{100}.

[c] No A_v from our observations.

[d] Properties listed are derived for $d = 100$ pc.

[e] Double entries in each row represent the properties of the extended MRN dust model and the population of small dust particles, respectively.

[f] Represented by the mass fraction of carbon locked up in PAHs. The cosmic value is 3.9×10^{-3} (Cameron 1982). Values calculated with $\sigma_{UV} = 10^{-15}$ cm^2/PAH, $F_{UV} = 8 \times 10^{-4}$ ergs cm^{-2} s^{-1} (see text).

summarizes these properties derived with a single dust temperature model. Values for the dust temperature are similar to those derived for cirrus associated with H I only (Low *et al.* 1984; Boulanger, Baud, and van Albada 1985); values for A_v/τ_{100} are also similar to those derived by Low *et al.* The very different gas content of the clouds with and without CO does not seem to be reflected in their observed dust properties.

The dust temperature for cloud 20 decreases from 25–26 K at the edges to 20–21 K at the center; within the uncertainties of the background subtraction, we find no significant temperature structure for clouds 16 and 30. The dust temperature gradient for cloud 20 could be understood as an UV optical depth effect under the assumption that the external radiation field is the dominant heating source for the cloud (see below). The CO observations of cloud 20, on the other hand, show an increase in peak antenna temperature toward the center of the cloud. Since the center of cloud 20 has the largest ^{13}CO optical depth of the three clouds, the increase in CO antenna temperature may be due to greater collisional coupling with the dust in the region of largest gas volume density.

For each of the three selected HLCs, we find a linear correlation between W(CO) and the 100 μm intensity (I_{100}) which is significant at a confidence level in excess of 99%. The slope of the regression, $W(\text{CO})/I_{100}$, is similar from cloud to cloud, with a mean value of 0.9 K km s^{-1} (MJy sr^{-1})$^{-1}$. This value is significantly higher than the value of ~ 0.05 K km s^{-1} (MJy sr^{-1})$^{-1}$ obtained by Hauser *et al.* (1984) in their survey of the central part of the Galaxy, and by Rickard and Harvey (1984) for a number of galaxies. The latter two studies measure the emission averaged over the bulk of the molecular cloud ensemble, indicating that the HLCs have anomalously large CO emission relative to the far-IR. The correlations show significantly nonzero I_{100} intercepts even though the IR zodiacal background has been removed, which may be attributed to dust associated with H I along the line of sight to the HLCs. Values for $W(\text{H I})/I_{100}$ obtained from these intercepts and velocity-integrated H I data (−45 to +45 km s^{-1}) from the Heiles and Habing (1974) survey are within a factor of 2 of the 39 K km s^{-1} (MJy sr^{-1})$^{-1}$ quoted by Boulanger, Baud, and van Albada (1985) for the H I/cirrus clouds they analyzed.

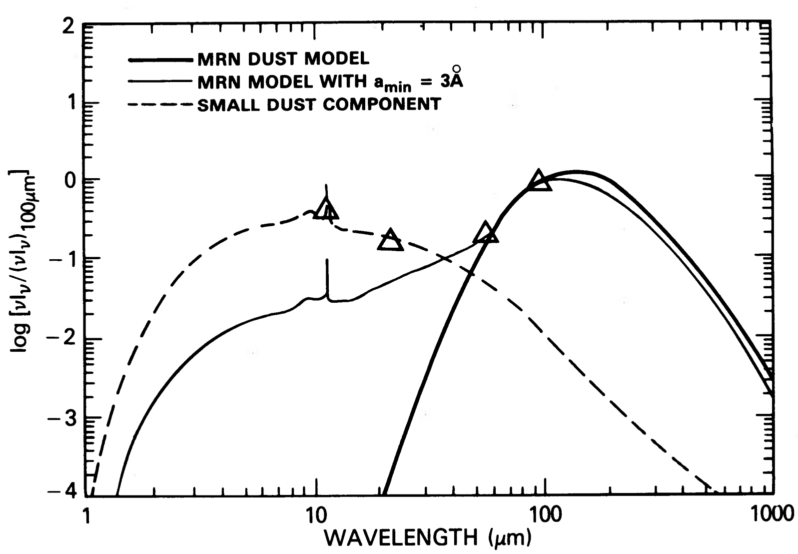

FIG. 2.—Model fitted to average *IRAS* energy distributions. Intensities for each cloud are normalized to its 100 μm intensity; normalized values for all three clouds are close enough that all are represented by the large triangle. Bold line is standard MRN model; thin solid line represents MRN extended down to 3 Å (see text). The small particle component (*dashed line*) is characterized by a size range a = 3–10 Å, with an a^{-5} distribution.

The three selected clouds have very similar infrared energy distributions. Figure 2 presents the average energy distribution of the three clouds, normalized to 100 μm intensity. Also shown in the figure are calculated infrared intensities for clouds having a "standard" Mathis, Rumpl, and Nordsieck (1977; hereafter MRN) graphite-silicate mixture of dust particles, and for clouds with an MRN distribution of grain sizes extended down to 3 Å. The dust was assumed to be heated by the interstellar radiation field (ISRF) as modeled by Mathis, Mezger, and Panagia (1983). Dust grains with sizes below 200 Å are stochastically heated by the ISRF (Draine and Anderson 1985); we calculate their temperature distribution using the model of Dwek (1986). Our calculations confirm the suggestion (e.g., Draine and Anderson 1985; Puget, Leger, and Boulanger 1986) that a component of very small dust particles is needed to explain the observed emission in the 12 and 25 μm *IRAS* bands. The grain size distribution of this component is constrained to be both narrow and steep in order to produce the observed 12 μm emission without adding excess 60 μm emission. Alternatively, the small grain component may be in the form of polycyclic aromatic hydrocarbons (PAHs; Leger and Puget 1984; Allamandola, Tielens, and Barker 1985, hereafter ATB). The observed infrared emission constrains the line excitation mechanism: if the mechanism is molecular (ATB), then for a reasonable UV photon absorption cross section σ_{UV}, and ISRF UV flux, F_{UV}, an uncomfortably large amount (half or more) of the interstellar carbon needs to be tied up in PAHs (see Table 2B). This fraction may be significantly smaller if the lines are thermally excited (Leger and Puget 1984).

Table 2B summarizes the properties of the three HLCs derived from the stochastic heating model. The total optical depth at 100 μm is about five times larger than that inferred from the assumption of a single dust temperature. About one-third of the dust mass and cloud luminosity is in the small particle component. Comparison of the dust masses with total cloud masses derived from the CO observation gives a gas-to-dust mass ratio of $\sim$ 100, typical of the general ISM. The total infrared luminosity per hydrogen mass for these clouds is about 2 ($L_\odot/M_\odot$), suggesting that there are no significant embedded heating sources (Hauser *et al.* 1984; Ryter and Puget 1977).

In summary, identification of some of the infrared cirrus with HLCs has clarified one mystery, and leads us to many intriguing questions. These include the following: (1) what induces transition between the two kinds of clouds (i.e., predominantly atomic vs. predominantly molecular)?; (2) why is CO/IR much larger in the HLCs than in the Galaxy and external galaxies generally?; and (3) what is the nature and evolutionary state of the "very small grain" component?

We gratefully acknowledge the support of the Sterrewacht Leiden for making their facilities available to us to produce the star count data, and of Cor de Vries who provided us with his excellent reduction programs. We also thank Richard A. White for his expert guidance in analyzing the *IRAS* images, and François Boulanger for helpful discussions. This work is partially supported by NSF grant AST 83-15726 and by NASA under the *IRAS* Extended Mission Program.

REFERENCES

Allamandola, L. J., Tielens, A. G. G. M., and Barker, J. R. 1985, *Ap. J.* (*Letters*), **290**, L25 (ATB).
Blitz, L., Magnani, L., and Mundy, L. 1984, *Ap. J.* (*Letters*), **282**, L9 (BMM).
Boulanger, F., Baud, B., and van Albada, T. 1985, *Astr. Ap.*, **144**, L9.
Cameron, A. G. W. 1982, in *Essays in Nuclear Astrophysics*, ed. C. A. Barnes, D. D. Clayton, and D. N. Schramm (Cambridge: Cambridge University Press), p. 23.
Draine, B. T., and Anderson, N. 1985, *Ap. J.*, **292**, 494.
Dwek, E. 1986, *Ap. J.*, **302**, 363.
Hauser, M. G., *et al.* 1984, *Ap. J.*, **285**, 74.
Heiles, C., and Habing, H. J. 1974, *Astr. Ap. Suppl.*, **14**, 1.
IRAS Explanatory Supplement. 1984, ed. C. A. Beichman, G. Neugebauer, H. J. Habing, P. E. Clegg, and T. J. Chester (Washington: Government Printing Office).
Keto, E., and Myers, P. 1986, *Ap. J.*, **304**, 466.
Leger, A., and Puget, J. L. 1984, *Astr. Ap.*, **137**, L5.
Low, F. J., *et al.* 1984, *Ap. J.* (*Letters*), **278**, L19.
Magnani, L., Blitz, L., and Mundy, L. 1985, *Ap. J.*, **295**, 402 (MBM).
Magnani, L., Blitz, L., and Wouterloot, J. G. A. 1986, in preparation.
Magnani, L., and de Vries, C. 1986, *Astr. Ap.*, submitted.
Mathis, J. S., Mezger, P. G., and Panagia, N. 1983, *Astr. Ap.*, **128**, 212.
Mathis, J. S., Rumpl, W., and Nordsieck, K. H. 1977, *Ap. J.*, **217**, 425.
Puget, J. L., Leger, A., and Boulanger, F. 1986, *Astr. Ap.*, in press.
Rickard, L. J, and Harvey, P. 1984, *A.J.*, **89**, 1520.
Ryter, C. E., and Puget, J. L. 1977, *Ap. J.*, **215**, 775.
Sandage, A. 1976, *A.J.*, **81**, 954.

LEO BLITZ and LORIS MAGNANI: Astronomy Program, University of Maryland, College Park, MD 20742

ELI DWEK and M. G. HAUSER: Code 697, Laboratory for Extraterrestrial Physics, Goddard Space Flight Center, Greenbelt, MD 20771

LEE J RICKARD: E. O. Hulburt Center for Space Research, Naval Research Laboratory, Code 4138R, Washington, DC 20375-5000

JANET L. WEILAND: Applied Research Corporation, 8201 Corporate Drive, Suite 920, Landover, MD 20785